southern Spain turns into desert, deciduous forests invade most of the mountains, and Mediterranean vegetation replaces most of the deciduous forests in a large part of the Mediterranean basin. Figure 3H illustrates the variation from areas without any changes, regardless of scenario (stable white areas), to areas in which changes from scenario RCP2.6 already appear (red areas). As expected, the most-sensitive areas are those located at the limit between two biomes—for example, in the mountains at the transition between temperate and montane forest or in the southern Mediterranean at the transition between forest and desert biomes. The map for 4700 yr B.P., in which the past changes were among the highest (Fig. 3B), has the largest changes in the southwest, eastern steppe areas, and the mountains, but these changes are relatively sparse.

Our analysis shows that, in approximately one century, anthropogenic climate change without ambitious mitigation policies will likely alter ecosystems in the Mediterranean in a way that is without precedent during the past 10 millennia. Despite known uncertainties in climate models, GHG emission scenarios at the level of country commitments before the UNFCCC Paris Agreement will likely lead to the substantial expansion of deserts in much of southern Europe and northern Africa. The highly ambitious RCP2.6 scenario seems to be the only possible pathway toward more limited impacts. Only the coldest RCP2.6L simulations, which correspond broadly to the 1.5°C target of the Paris Agreement, allow ecosystem shifts to remain inside the limits experienced during the Holocene.

This analysis does not account for other human impacts on ecosystems, in addition to climate change (i.e., land-use change, urbanization, soil degradation, etc.), which have grown in importance after the mid-Holocene and have become dominant during the past centuries. Many of these effects are likely to become even stronger in the future because of the expanding human population and economic activity. Most land change processes reduce natural vegetation or they seal or degrade the soils, representing additional effects on ecosystems, which will enhance, rather than dampen, the biome shifts toward a drier state than estimated by this analysis. This assessment shows that, without ambitious climate targets, the potential for future managed or unmanaged ecosystems to host biodiversity or deliver services to society is likely to be greatly reduced by climate change and direct local effects.

REFERENCES AND NOTES

1. S. I. Seneviratne, M. G. Donat, A. J. Pitman, R. Knutti, R. L. Wilby, *Nature* **529**, 477–483 (2016).
2. W. Cramer *et al.*, in *Climate Change 2014: Impacts, Adaptation, and Vulnerability. Part A: Global and Sectoral Aspects. Contribution of Working Group II to the Fifth Assessment Report of the Intergovernmental Panel on Climate Change*, C. B. Field *et al.*, Eds. (Cambridge Univ. Press, 2014), pp. 979–1037.
3. C.-F. Schleussner *et al.*, *Earth Syst. Dyn. Discuss.* **6**, 2447–2505 (2015).
4. J. Guiot, D. Kaniewski, *Front. Earth Sci.* **3**, 28 (2015).
5. F. Médail, N. Myers, in *Hotspots Revisited: Earth's Biologically Richest and Most Endangered Terrestrial Ecoregions*, R. A. Mittermeier *et al.*, Eds. (Conservation International, 2004), pp. 144–147.
6. Materials and methods are available as supplementary materials on *Science* Online.
7. E. Xoplaki, J. F. González-Rouco, J. Luterbacher, H. Wanner, *Clim. Dyn.* **23**, 63–78 (2004).
8. L. Maiorano *et al.*, *Philos. Trans. R. Soc. London Ser. B* **366**, 2681–2692 (2011).
9. T. Keenan, J. Maria Serra, F. Lloret, M. Ninyerola, S. Sabate, *Glob. Change Biol.* **17**, 565–579 (2011).
10. W. Thuiller, S. Lavorel, M. B. Araújo, *Glob. Ecol. Biogeogr.* **14**, 347–357 (2005).
11. B. Weninger *et al.*, *Doc. Praehist.* **36**, 7–59 (2009).
12. D. Kaniewski, E. Van Campo, H. Weiss, *Proc. Natl. Acad. Sci. U.S.A.* **109**, 3862–3867 (2012).
13. N. Roberts, D. Brayshaw, C. Kuzucuoglu, R. Perez, L. Sadori, *Holocene* **21**, 3–13 (2011).
14. C. P. Kelley, S. Mohtadi, M. A. Cane, R. Seager, Y. Kushnir, *Proc. Natl. Acad. Sci. U.S.A.* **112**, 3241–3246 (2015).
15. B. I. Cook, K. J. Anchukaitis, R. Touchan, D. M. Meko, E. R. Cook, *J. Geophys. Res.* **121**, 2060–2074 (2016).
16. G. Middleton, *J. Archaeol. Res.* **20**, 257–307 (2012).
17. A. B. Knapp, S. W. Manning, *Am. J. Archaeol.* **120**, 99–149 (2016).
18. C. B. Yackulc, J. D. Nichols, J. Reid, R. Der, *Ecology* **96**, 16–23 (2015).
19. C. Roumieux *et al.*, *Ecol. Mediterr.* **36**, 17–24 (2010).
20. I. Harris, P. D. Jones, T. J. Osborn, D. H. Lister, *Int. J. Climatol.* **34**, 623–642 (2014).

ACKNOWLEDGMENTS

The authors are members of the Observatoire des Sciences de l'Univers Pytheas Institute and the ECCOREV network. This research has been funded by Labex OT-Med (project ANR-11-LABEX-0061), the "Investissements d'Avenir" French government project of the French National Research Agency (ANR), AMidex (project 11-IDEX-0001-02), and the European Union FP7-ENVIRONMENT project OPERAs (grant 308393). We acknowledge the World Climate Research Programme's Working Group on Coupled Modelling, which is responsible for CMIP, and we thank the climate modeling groups (table S2) for producing and making their model outputs available. For CMIP, the U.S. Department of Energy's Program for Climate Model Diagnosis and Intercomparison provides coordinating support and led the development of software infrastructure, in partnership with the Global Organization for Earth System Science Portals. R. Suarez and S. Shi have extracted and preprocessed the model simulations. Holocene climate reconstructions are available at http://database.otmed.fr/geonetworkotmed/srv/eng/search - |54b9bf34-57ae-45ea-b455-9f90351e538f. Future climate projections are available at http://cmip-pcmdi.llnl.gov/cmip5/.

SUPPLEMENTARY MATERIALS

www.sciencemag.org/content/354/6311/465/suppl/DC1
Materials and Methods
Table S1 and S2
References (*21*–*28*)

6 July 2016; accepted 21 September 2016
10.1126/science.aah5015

GENE EXPRESSION

Xist recruits the X chromosome to the nuclear lamina to enable chromosome-wide silencing

Chun-Kan Chen,[1] Mario Blanco,[1] Constanza Jackson,[1] Erik Aznauryan,[1] Noah Ollikainen,[1] Christine Surka,[1] Amy Chow,[1] Andrea Cerase,[2] Patrick McDonel,[3] Mitchell Guttman[1]*

The Xist long noncoding RNA orchestrates X chromosome inactivation, a process that entails chromosome-wide silencing and remodeling of the three-dimensional (3D) structure of the X chromosome. Yet, it remains unclear whether these changes in nuclear structure are mediated by Xist and whether they are required for silencing. Here, we show that Xist directly interacts with the Lamin B receptor, an integral component of the nuclear lamina, and that this interaction is required for Xist-mediated silencing by recruiting the inactive X to the nuclear lamina and by doing so enables Xist to spread to actively transcribed genes across the X. Our results demonstrate that lamina recruitment changes the 3D structure of DNA, enabling Xist and its silencing proteins to spread across the X to silence transcription.

The Xist long noncoding RNA (lncRNA) initiates X chromosome inactivation (XCI), a process that entails chromosome-wide transcriptional silencing (*1*) and large-scale remodeling of the three-dimensional (3D) structure of the X chromosome (*2*–*4*), by spreading across the future inactive X chromosome and excluding RNA polymerase II (PolII) (*1*, *5*). Xist initially localizes to genomic DNA regions on the X chromosome that are not actively transcribed (*6*–*8*), before spreading to actively transcribed genes (*7*–*9*). Deletion of a highly conserved region of Xist that is required for transcriptional silencing, called the A-repeat (*10*), leads to a defect in Xist spreading (*7*) and spatial exclusion of active genes from the Xist-coated nuclear compartment (*9*). Whether these structural changes are required for, or merely a consequence of, transcriptional silencing mediated by the A-repeat of Xist remains unclear (*7*, *9*). Recently, we and others identified by means of mass spectrometry the proteins that interact with Xist (*11*–*13*). One of these proteins is the Lamin B receptor (LBR) (*11*, *13*), a transmembrane protein that is anchored in the inner nuclear membrane, binds to Lamin B,

and is required for anchoring chromatin to the nuclear lamina (*14*)—a nuclear compartment that helps shape the 3D structure of DNA (*15*) and is enriched for silencing proteins (*14*, *16*). Because induction of XCI leads to recruitment of the inactive X-chromosome to the nuclear lamina (*4*), we hypothesized that the Xist-LBR interaction might be required to shape nuclear structure and regulate gene expression during XCI.

To test this, we knocked down LBR and measured the expression of five X chromosome genes and two autosomal genes before and after Xist induction (supplementary materials, materials and methods, note 1). Knockdown of LBR led to a defect in Xist-mediated silencing of these X chromosome genes but showed no effect on autosomal genes (Fig. 1A and figs. S1 and S2). We observed a similar silencing defect upon knockdown or knockout of LBR in differentiating female embryonic stem cells (fig. S3 and note 2). This silencing defect is not merely caused by disruption of the nuclear lamina because knockdown of Lamin B1 or Emerin, additional components of the nuclear lamina (*14*), had no effect on Xist-mediated silencing (Fig. 1A and fig. S4).

We hypothesized that the arginine-serine (RS) motif of LBR might be required for interacting with Xist (fig. S4A and note 3). A truncated LBR protein containing a deletion of the RS motif (ΔRS-LBR) (fig. S5 and materials and methods) did not interact with Xist (~97% reduced binding) (Fig. 1B and materials and methods) and failed to rescue the silencing defect upon knockdown of LBR (Fig. 1C and figs. S1B and S6). In contrast, deletion of seven of the eight transmembrane domains (ΔTM-LBR) (fig. S5) did not affect Xist binding (Fig. 1B) and was able to rescue the silencing defect upon knockdown of LBR (Fig. 1C, figs. S1B and S6, and note 4). To ensure that ΔRS-LBR fails to silence X chromosome genes because of its RNA binding ability, we fused three copies of the viral BoxB RNA aptamer, which binds tightly to the viral λN coat protein (*17*), to the 3′ end of the endogenous Xist RNA (Xist-BoxB) (fig. S7). Expression of ΔRS-LBR-λN in Xist-BoxB cells rescued the silencing defect observed upon LBR knockdown (Fig. 1D). Together, these results demonstrate that the Xist-LBR interaction is required for Xist-mediated transcriptional silencing.

We identified three discrete LBR binding sites (LBSs) that are spread across >10,000 nucleotides of the Xist RNA (Fig. 2A and materials and methods, note 5). One LBR binding site (LBS-1) overlaps the ~900 nucleotide region of Xist required for silencing (ΔA-repeat region) (Fig. 2A) (*10*). We tested LBR binding within a ΔA-repeat cell line (*10*) and found that LBR binding is disrupted across the entire Xist RNA (Fig. 2B), including the LBR binding sites that do not overlap the ΔA-repeat region (fig. S8). Because the Xist-binding protein SMRT/HDAC1–associated repressor protein (SHARP, also called Spen) also binds within the ΔA-repeat region (Fig. 2A) (*12*, *18*) and its binding is also disrupted in ΔA-Xist (Fig. 2B) (*12*), we generated a mutant Xist that precisely deletes a region within the LBR binding site that is not within the SHARP binding site (ΔLBS-Xist) (Fig. 2A). In ΔLBS-Xist, LBR binding was lost across the entire Xist RNA without affecting SHARP binding (Fig. 2B and fig. S8). ΔLBS-Xist fails to silence X chromosome transcription to a similar level, as observed in the ΔA-Xist (Fig. 2C, figs. S1 and S9, and notes 6 and 7).

To ensure that the observed silencing defect in ΔLBS-Xist cells is due to LBR-binding alone and not disruption of another unknown protein interaction, we tested whether we could rescue the observed silencing defect by reestablishing the ΔLBS-LBR interaction. To do this, we generated an endogenous ΔLBS-BoxB Xist RNA (materials and methods) and confirmed that expression of LBR-λN, but not LBR fused to a different RNA-binding domain (MS2-coat protein) (*19*), was able to rescue the silencing defect observed in ΔLBS-BoxB cells (Fig. 2D, fig. S10, and materials and methods). In contrast, expression of other silencing proteins fused to λN, such as SHARP and embryonic ectoderm development (EED), did not rescue the observed silencing defect (Fig. 2D and fig. S11), demonstrating that the LBR-binding site that overlaps the ΔA-repeat region of Xist is required for silencing.

We hypothesized that the Xist-LBR interaction might be required for recruiting the inactive X chromosome to the nuclear lamina (*4*). To test this, we measured the distance between the Xist-coated nuclear compartment and Lamin B1 in the nucleus using RNA fluorescence in situ hybridization (FISH), X chromosome paint, and immunofluorescence (fig. S12A and materials and methods). Upon Xist induction in wild-type cells, we found that the Xist compartment overlaps Lamin B1 signal (~90% of cells) (Fig. 3A, figs. S12 and S13, and note 8). In contrast, upon LBR knockdown or knockout, ΔLBS-Xist, or ΔA-Xist cells, there was a clear separation between the Xist-coated compartment and Lamin B1, demonstrating a >20-fold increase in distance relative to wild-type Xist (Fig. 3 and figs. S12 and S13). Thus, recruitment of the inactive X chromosome to the nuclear lamina is directly mediated by the Xist RNA through its interaction with LBR.

To determine whether LBR-mediated recruitment of the X chromosome to the nuclear lamina leads to Xist-mediated transcriptional silencing, we replaced the Xist-LBR interaction with another protein that interacts with the nuclear lamina; specifically, we used our endogenous ΔLBS-BoxB Xist, which fails to interact with LBR,

[1]Division of Biology and Biological Engineering, California Institute of Technology, Pasadena, CA 91125, USA. [2]European Molecular Biology Laboratory–Monterotondo, Via Ramarini 32, 00015 Monterotondo (RM), Italy. [3]Program in Molecular Medicine, University of Massachusetts Medical School, Worcester, MA 01655, USA.
*Corresponding author. Email: mguttman@caltech.edu

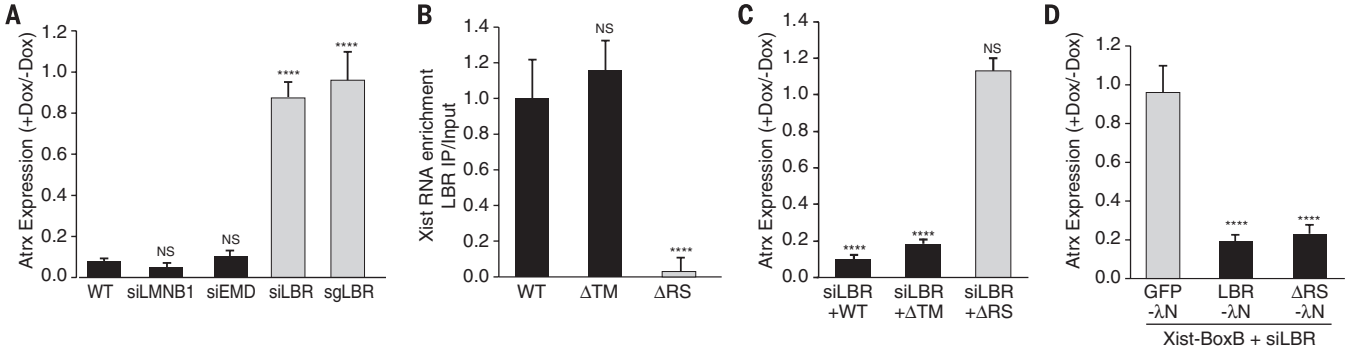

Fig. 1. LBR requires its RS motif to interact with Xist and silence transcription. (**A**) Atrx mRNA levels after Xist induction (+dox) relative to pre-Xist (−dox) levels upon knockdown of various nuclear lamina proteins. WT, scrambled small interfering RNA (siRNA) control; siEMD, Emerin knockdown; siLMNB1, Lamin B1 knockdown; sgLBR, knockdown of LBR by using dCas9-KRAB (materials and methods). (**B**) Xist enrichment after immunoprecipitation of a 3x-FLAG–tagged full-length LBR (WT), ΔRS-LBR, or ΔTM-LBR (materials and methods). Error bars indicate SEM from three independent IP experiments. (**C**) Relative Atrx mRNA expression upon knockdown of the endogenous LBR and expression of full length LBR (WT), ΔTM-LBR, or ΔRS-LBR. (**D**) Relative Atrx mRNA expression in Xist-BoxB cells after knockdown of the endogenous LBR and expression of green fluorescent protein (GFP)–λN (control), LBR-λN, or ΔRS-LBR-λN. NS, not significant. ****$P < 0.001$ relative to [(A) and (B)] wild-type cells, (C) cells transfected with siRNAs alone [shown in (A)], or (D) cells transfected with GFP-λN by means of an unpaired two-sample *t* test. Error bars indicate SEM across 50 individual cells.

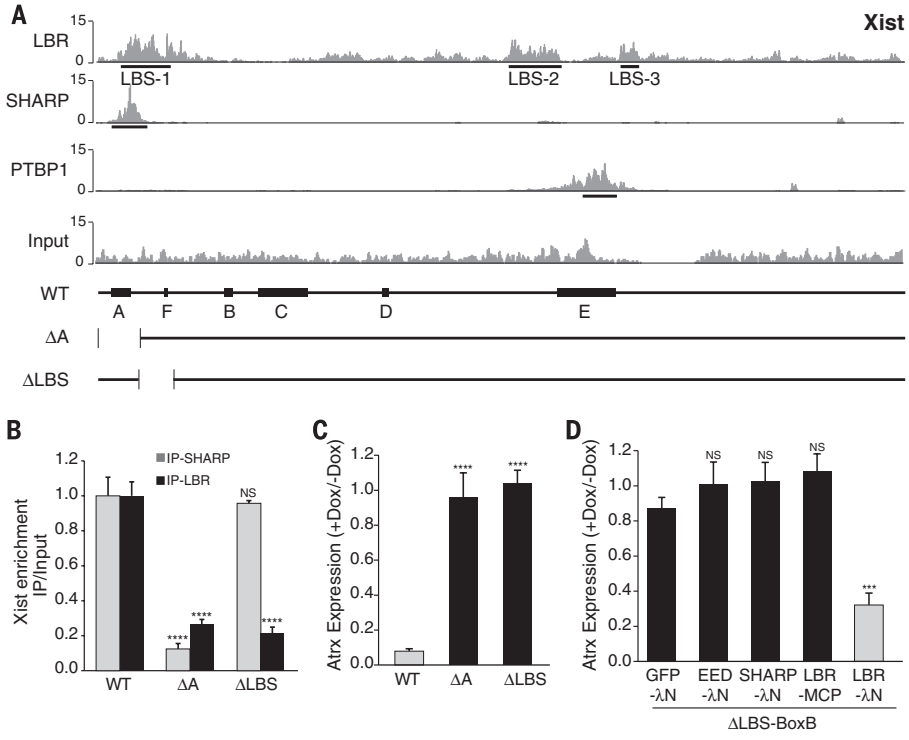

Fig. 2. LBR binds to precise regions of the Xist RNA that are required for silencing. (**A**) Cross-linking immunoprecipitation (CLIP) data plotted across the Xist RNA for LBR, SHARP, and PTBP1 proteins. The values represent fold-enrichment at each position on Xist normalized to a size-matched input RNA control. Input represents the total RNA control for the LBR sample. (Bottom) A schematic of the annotated repeat regions on the Xist RNA (WT) and the locations of the deleted regions in ΔA (nucleotides 1–937) and ΔLBS (nucleotides 898–1682). (**B**) Xist RNA enrichment level measured with quantitative reverse transcription polymerase chain reaction after immunoprecipitation of endogenous LBR or SHARP in wild-type, ΔA, or ΔLBS cells. Error bars indicate SEM from four independent immunoprecipitation experiments. (**C**) Relative Atrx mRNA expression in wild-type, ΔA, or ΔLBS-Xist cells. (**D**) Expression of ΔLBS-Xist with a 3x-BoxB fusion (ΔLBS-BoxB) along with expression of GFP-λN (control), EED-λN, SHARP-λN, or LBR-λN. As an additional control, we expressed LBR fused with the bacteriophage MS2 coat protein (LBR-MCP). Error bars indicate SEM across 50 individual cells. NS, not significant. ***$P < 0.005$, ****$P < 0.001$ relative to wild-type cells [(B) and (C)], or cells transfected with GFP-λN (D) by means of an unpaired two-sample *t* test.

to create an interaction between Xist and Lamin B1 (fig. S14A). We expressed a Lamin B1-λN fusion protein and confirmed that in cells expressing ΔLBS-BoxB Xist, the Xist-compartment was recruited to the nuclear lamina to a similar extent as that observed in wild-type conditions (Fig. 3, A and B, and fig. S12). Tethering Xist to the nuclear lamina rescues the Xist-silencing defect observed in ΔLBS cells to the same extent as that observed after rescuing directly with LBR-λN (Fig. 3C and fig. S14). Thus, Xist-mediated recruitment of the X chromosome to the nuclear lamina is required for Xist-mediated transcriptional silencing, and the function of LBR in Xist-mediated silencing is to recruit the X chromosome to the nuclear lamina.

We considered the possibility that recruitment to the nuclear lamina, a nuclear territory enriched for silenced DNA and repressive chromatin regulators (*14*, *16*), may act to directly silence transcription on the X chromosome (*20*, *21*). To test this, we knocked down SHARP, which fails to silence transcription on the X chromosome (*11*, *12*, *18*, *22*), and observed that the Xist-coated compartment was still localized at the nuclear lamina, demonstrating a comparable distance distribution between Xist and Lamin B1 to that observed for wild-type Xist (Fig. 3, A and B, and fig. S12). Therefore, Xist-mediated recruitment of the X chromosome to the nuclear lamina does not directly lead to transcriptional silencing because the X chromosome can still be transcribed even when localized at the nuclear lamina.

Instead, we considered the possibility that LBR-mediated recruitment of the X chromosome to the nuclear lamina could reposition active genes into the Xist-coated nuclear compartment, allowing Xist to spread across the X chromosome. Indeed, the Xist RNA gradually localizes to genes that are actively transcribed before initiation of XCI (*7*), but deletion of the A-repeat leads to a

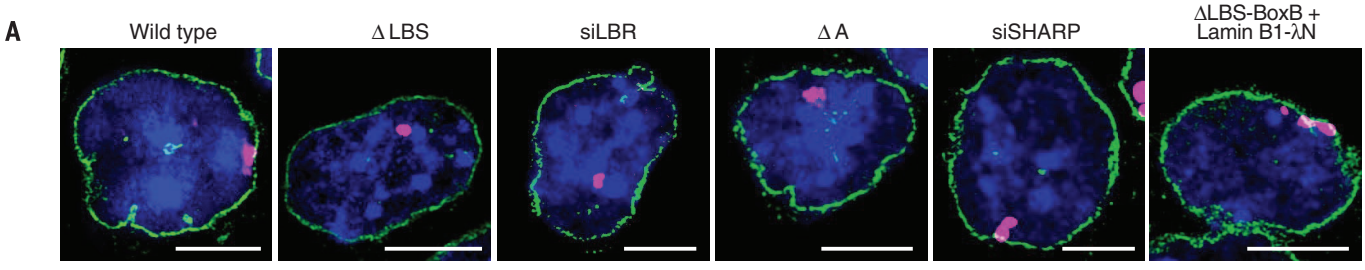

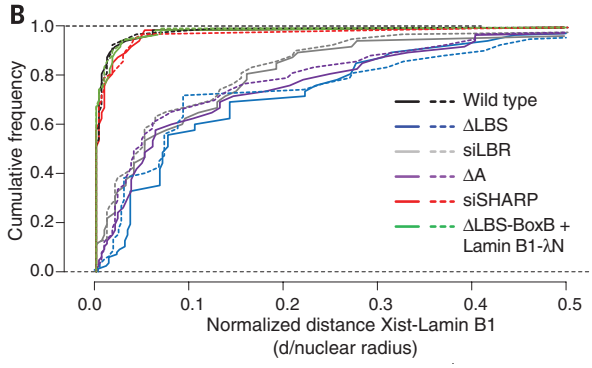

Fig. 3. Xist-mediated recruitment of DNA to the nuclear lamina is required for transcriptional silencing. (**A**) Images of Xist (red), Lamin B1 (green), and 4′,6-diamidino-2-phenylindole (DAPI) (blue) across different conditions. Scale bars, 5 μm. (**B**) The cumulative frequency distribution of normalized distances between Xist and Lamin B1 across 40 individual cells across different conditions. Dashed lines represents a second independent experiment. (**C**) Relative Atrx mRNA expression in ΔLBS-BoxB cells along with expression of LBR-MCP (control), LBR-λN, or LaminB1-λN. Error bars indicate SEM across 50 individual cells. NS, not significant. ****$P < 0.001$ relative to cells transfected with LBR-MCP by means of an unpaired two-sample *t* test.

defect in Xist spreading to these actively transcribed regions (*7*, *9*). In ΔLBS-Xist cells or upon knockdown of LBR, we observed a strong depletion of Xist RNA localization across regions of actively transcribed genes, comparable with the defect observed in ΔA-Xist cells (Fig. 4, A and B, and figs. S15 and S16) (*7*). We found that Xist RNA localization is even more strongly depleted over more highly transcribed genes (Fig. 4B). Knockdown of SHARP, which also binds the A-repeat, did not affect Xist localization (Fig. 4B and fig. S15). Synthetically tethering ΔLBS-BoxB to the nuclear lamina by using a Lamin B1-λN fusion enables Xist to spread to active genes to a similar level as that observed in wild-type conditions (Fig. 4B and figs. S15 and S16).

To determine whether this spreading defect is due to a failure to reposition actively transcribed genes into the Xist-coated compartment, we measured the position of the genomic loci of three actively transcribed genes relative to the Xist-coated compartment (Fig. 4C and materials and methods, note 9). In ΔLBS cells or upon knockdown or knockout of LBR, the distance between the Xist compartment and the loci of these actively transcribed X chromosome genes (Gpc4, Mecp2, and Pgk1 loci) were comparable with the distance between Xist and an autosomal gene (Notch2 locus) (Fig. 4, D and E, and figs. S17 and S18). Upon knockdown of SHARP, we found that these actively transcribed loci overlapped the Xist compartment (~80% of cells) (fig. S17), comparable with the Xist genomic locus itself (~90% of cells) (fig. S17). Because Xist can still spread to active genes upon knockdown of SHARP, which is known to be required for the exclusion of RNA PolII (*11*), our results demonstrate that spreading to active genes and exclusion of RNA PolII are independent functions that are both required for chromosome-wide transcriptional silencing.

Our results suggest a model for how Xist shapes the 3D nuclear structure of the inactive X chromosome to spread to active genes and silence chromosome-wide transcription (Fig. 4F and fig. S19). Xist initially localizes to the core of the X chromosome territory by localizing at DNA sites that are in close 3D proximity to its transcriptional locus (*7*). These initial Xist localization sites are generally inactive before Xist induction (*6*, *7*, *9*). The Xist-coated DNA, like other chromosomal DNA regions, will dynamically sample different nuclear locations (*23*) and, because Xist binds LBR, will become tethered at the nuclear lamina when it comes into spatial proximity. This lamina association is known to constrain chromosomal mobility

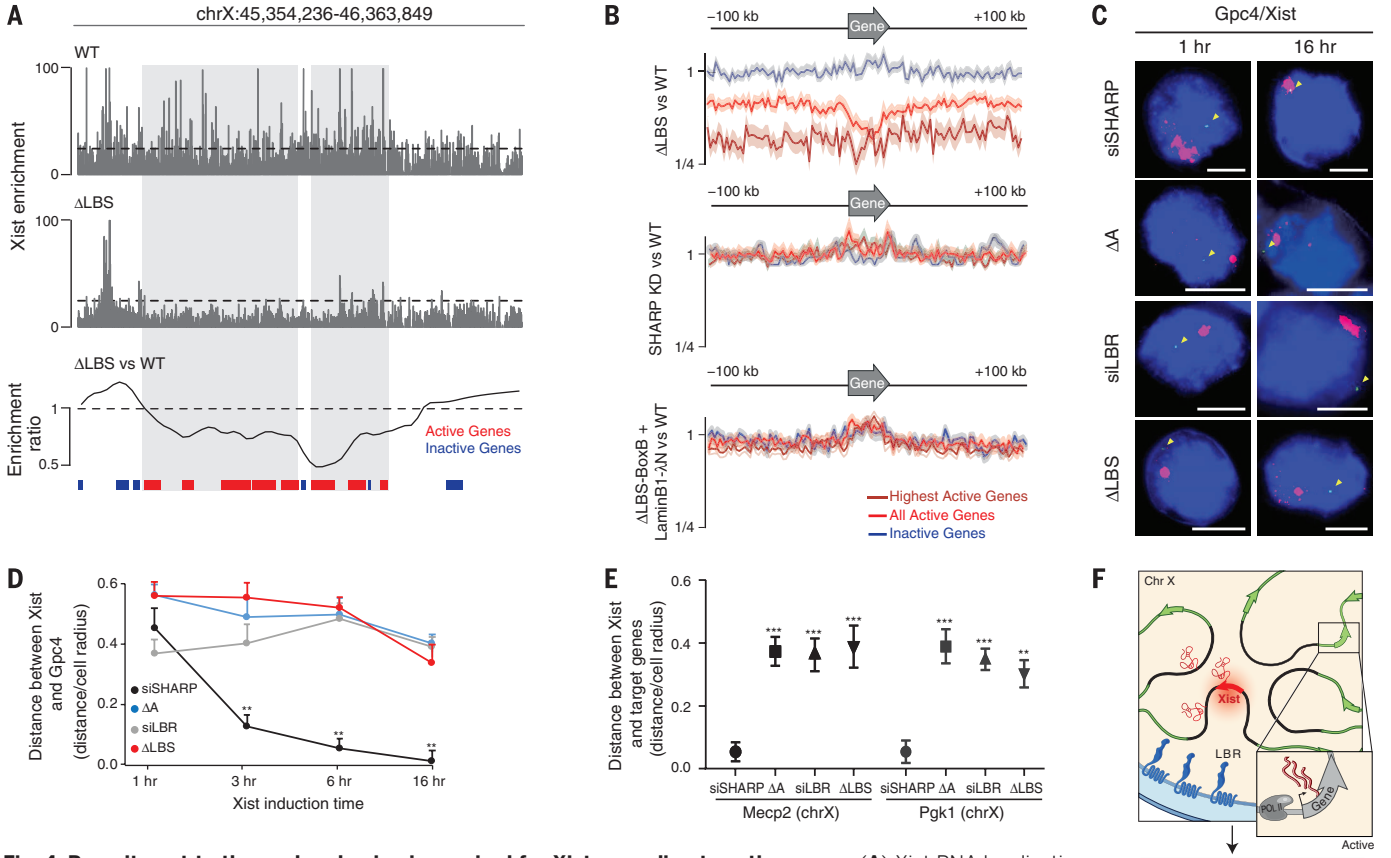

Fig. 4. Recruitment to the nuclear lamina is required for Xist spreading to active genes. (**A**) Xist RNA localization as measured with RNA antisense purification (RAP)–DNA for wild type (top), ΔLBS-Xist (middle), and the smoothed fold change (bottom) across a region of the X chromosome containing active (red) and inactive (blue) genes. The dashed line indicates average Xist enrichment in wild-type cells. (**B**) Aggregate Xist enrichment relative to the genomic locations of highly active genes [dark red, reads per kilobase per million (RPKM) > 5], all active genes (red, RPKM > 1), and inactive genes (blue) on the X-chromosome for ΔLBS, SHARP knockdown, and ΔLBS-BoxB + LMNB1-λN cells compared with wild-type cells. Shaded areas represent 95% confidence interval. (**C**) Images of Xist (red), Gpc4 locus (green), and DAPI (blue) across different cell lines (rows) after Xist induction for 1 or 16 hours. Yellow arrowheads indicate the genomic DNA location of Gpc4. Scale bars, 5 μm. (**D**) The median distance from Gpc4 locus to the Xist-compartment after Xist induction for 1, 3, 6, and 16 hours. Error bars represent the standard error of the median across 50 individual cells. $^{**}P < 0.01$ relative to 1-hour induction by means of an unpaired two-sample *t* test. (**E**) The median distance from the Mecp2 and Pgk1 locus to the Xist compartment after Xist induction for 16 hours across different conditions. Error bars represent the standard error of the median across 50 individual cells. $^{**}P < 0.01$, $^{***}P < 0.005$ relative to siRNAs targeting SHARP (siSHARP) by means of an unpaired two-sample *t* test. (**F**) A model for how Xist-mediated recruitment to the nuclear lamina enables spreading to active genes and transcriptional silencing on the X chromosome.

(*24*) and by doing so would position the Xist-coated DNA away from the actively transcribed Xist transcription locus. This would enable other DNA regions on the X chromosome, which are physically linked to these tethered regions, to be brought into closer spatial proximity of the Xist transcription locus. In this way, Xist and its silencing factors can spread to these newly accessible DNA regions on the X chromosome.

REFERENCES AND NOTES

1. R. Galupa, E. Heard, *Curr. Opin. Genet. Dev.* **31**, 57–66 (2015).
2. E. Splinter *et al.*, *Genes Dev.* **25**, 1371–1383 (2011).
3. S. S. Rao *et al.*, *Cell* **159**, 1665–1680 (2014).
4. A. Rego, P. B. Sinclair, W. Tao, I. Kireev, A. S. Belmont, *J. Cell Sci.* **121**, 1119–1127 (2008).
5. A. Wutz, *Nat. Rev. Genet.* **12**, 542–553 (2011).
6. C. M. Clemson, L. L. Hall, M. Byron, J. McNeil, J. B. Lawrence, *Proc. Natl. Acad. Sci. U.S.A.* **103**, 7688–7693 (2006).
7. J. M. Engreitz *et al.*, *Science* **341**, 1237973 (2013).
8. M. D. Simon *et al.*, *Nature* **504**, 465–469 (2013).
9. J. Chaumeil, P. Le Baccon, A. Wutz, E. Heard, *Genes Dev.* **20**, 2223–2237 (2006).
10. A. Wutz, T. P. Rasmussen, R. Jaenisch, *Nat. Genet.* **30**, 167–174 (2002).
11. C. A. McHugh *et al.*, *Nature* **521**, 232–236 (2015).
12. C. Chu *et al.*, *Cell* **161**, 404–416 (2015).
13. A. Minajigi *et al.*, *Science* **349**, aab2276 (2015).
14. Y. Gruenbaum, A. Margalit, R. D. Goldman, D. K. Shumaker, K. L. Wilson, *Nat. Rev. Mol. Cell Biol.* **6**, 21–31 (2005).
15. A. Pombo, N. Dillon, *Nat. Rev. Mol. Cell Biol.* **16**, 245–257 (2015).
16. J. Kind, B. van Steensel, *Curr. Opin. Cell Biol.* **22**, 320–325 (2010).
17. J. Baron-Benhamou, N. H. Gehring, A. E. Kulozik, M. W. Hentze, *Methods Mol. Biol.* **257**, 135–154 (2004).
18. A. Monfort *et al.*, *Cell Reports* **12**, 554–561 (2015).
19. A. R. Buxbaum, G. Haimovich, R. H. Singer, *Nat. Rev. Mol. Cell Biol.* **16**, 95–109 (2015).
20. L. E. Finlan *et al.*, *PLOS Genet.* **4**, e1000039 (2008).
21. K. L. Reddy, J. M. Zullo, E. Bertolino, H. Singh, *Nature* **452**, 243–247 (2008).
22. B. Moindrot *et al.*, *Cell Rep.* 10.1016/j.celrep.2015.06.053 (2015).
23. W. F. Marshall *et al.*, *Curr. Biol.* **7**, 930–939 (1997).
24. J. R. Chubb, S. Boyle, P. Perry, W. A. Bickmore, *Curr. Biol.* **12**, 439–445 (2002).

ACKNOWLEDGMENTS

We thank K. Plath for extensive discussions; A. Collazo for microscopy help; A. Shur, P. Quintero, and V. Grishkevich for technical help; M. Lai for analytical help; J. Engreitz, S. Quinodoz, M. Garber, I. Amit, and J. Rinn for comments on the manuscript; and S. Knemeyer for illustrations. Imaging was performed in the Biological Imaging Facility, and sequencing was performed in the Millard and Muriel Jacobs Genetics and Genomics Laboratory at the California Institute of Technology. C.-K.C. is supported by a NIH National Research Service Award training grant (T32GM07616). This research was funded by the New York Stem Cell Foundation, a NIH Director's Early Independence Award (DP5OD012190), the Edward Mallinckrodt Foundation, Sontag Foundation, Searle Scholars Program, Pew-Steward Scholars program, and funds from the California Institute of Technology. M.G. is a New York Stem Cell Foundation–Robertson Investigator. Sequencing data are available online from the National Center for Biotechnology Information Gene Expression Omnibus (www.ncbi.nlm.nih.gov/geo) accession no. GSE80510 (RAP data) and GSE86250 (CLIP data), and additional data and information are available at www.lncRNA.caltech.edu/data.php.

SUPPLEMENTARY MATERIALS

www.sciencemag.org/content/354/6311/468/suppl/DC1
Materials and Methods
Supplementary Text
Figs. S1 to S19
References (*25*–*49*)

5 December 2015; accepted 25 July 2016
Published online 4 August 2016
10.1126/science.aae0047

VASCULAR DISEASE

Senescent intimal foam cells are deleterious at all stages of atherosclerosis

Bennett G. Childs,[1] Darren J. Baker,[2] Tobias Wijshake,[2,3] Cheryl A. Conover,[4] Judith Campisi,[5,6] Jan M. van Deursen[1,2]*

Advanced atherosclerotic lesions contain senescent cells, but the role of these cells in atherogenesis remains unclear. Using transgenic and pharmacological approaches to eliminate senescent cells in atherosclerosis-prone low-density lipoprotein receptor–deficient (*Ldlr*$^{-/-}$) mice, we show that these cells are detrimental throughout disease pathogenesis. We find that foamy macrophages with senescence markers accumulate in the subendothelial space at the onset of atherosclerosis, where they drive pathology by increasing expression of key atherogenic and inflammatory cytokines and chemokines. In advanced lesions, senescent cells promote features of plaque instability, including elastic fiber degradation and fibrous cap thinning, by heightening metalloprotease production. Together, these results demonstrate that senescent cells are key drivers of atheroma formation and maturation and suggest that selective clearance of these cells by senolytic agents holds promise for the treatment of atherosclerosis.

Atherosclerosis initiates when oxidized lipoprotein infiltrates the subendothelial space of arteries, often due to aberrantly elevated levels of apolipoprotein B–containing lipoproteins in the blood (*1*). Chemotactic signals arising from activated endothelium and vascular smooth muscle attract circulating monocytes that develop into lipid-loaded foamy macrophages, a subset of which adopt a proinflammatory phenotype through a mechanism that is not fully understood. The proinflammatory signals lead to additional rounds of monocyte recruitment and accumulation of other inflammatory cells (including T and B cells, dendritic cells, and mast cells), allowing initial lesions, often termed "fatty streaks," to increase in size and develop into plaques (*2*). Plaque stability, rather than absolute size, determines whether atherosclerosis is clinically silent or pathogenic because unstable plaques can rupture and produce vessel-occluding thrombosis and end-organ damage. Stable plaques have a relatively thick fibrous cap, which largely consists of vascular smooth muscle cells (VSMCs) and extracellular matrix components, partitioning soluble clotting factors in the blood from thrombogenic molecules in the plaque (*3*). In advanced disease, plaques destabilize when elevated local matrix metalloprotease production degrades the fibrous cap, increasing the risk of lesion rupture and subsequent thrombosis.

Advanced plaques contain cells with markers of senescence, a stress response that entails a permanent growth arrest coupled to the robust secretion of numerous biologically active molecules and is referred to as the senescence-associated secretory phenotype (SASP). The senescence markers include elevated senescence-associated β-galactosidase (SA β-Gal) activity and $p16^{Ink4a}$, p53, and p21 expression (*4*, *5*). However, whether and how senescent cells contribute to atherogenesis remains unclear (*6*, *7*). Human plaques contain cells with shortened telomeres, which predispose cells to undergo senescence (*8*). Consistent with a proatherogenic role of senescence is the observation that expression of a loss-of-function telomere-binding protein (Trf2) in VSMCs accelerates plaque growth in the *ApoE*$^{-/-}$ mouse model of atherosclerosis, although in vivo evidence for increased senescence in plaques was not provided. On the other hand, mice lacking core components of senescence pathways, such as p53, p21, or $p19^{Arf}$ (*7*, *9*–*11*), show accelerated atherosclerosis, implying a protective role for senescence. Studies showing that human and mouse polymorphisms that reduce expression of $p16^{Ink4a}$ and $p14^{Arf}$ ($p19^{Arf}$ in mice) correlate with increased atheroma risk support this conclusion (*7*, *12*, *13*). Thus, whether senescent cells accelerate or retard atherogenesis is unclear.

We used genetic and pharmacological methods of eliminating senescent cells to examine the role of naturally occurring senescent cells at different stages of atherogenesis. First, we verified that senescent cells accumulate in low-density lipoprotein receptor–deficient (*Ldlr*$^{-/-}$) mice, a model of atherogenesis. We fed 10-week-old *Ldlr*$^{-/-}$ mice a high-fat diet (HFD) for 88 days. We then performed SA β-Gal staining, which

[1]Department of Biochemistry and Molecular Biology, Mayo Clinic, Rochester, MN 55905, USA. [2]Department of Pediatric and Adolescent Medicine, Mayo Clinic, Rochester, MN 55905, USA. [3]Department of Pediatrics, University of Groningen, University Medical Center Groningen, 9713 AV Groningen, Netherlands. [4]Division of Endocrinology, Metabolism, and Nutrition, Mayo Clinic, Rochester, MN 55905, USA. [5]Buck Institute for Research on Aging, Novato, CA 94945, USA. [6]Life Sciences Division, Lawrence Berkeley National Laboratory, Berkeley, CA 94720, USA.
*Corresponding author. Email: vandeursen.jan@mayo.edu

Science

Xist recruits the X chromosome to the nuclear lamina to enable chromosome-wide silencing

Chun-Kan Chen, Mario Blanco, Constanza Jackson, Erik Aznauryan, Noah Ollikainen, Christine Surka, Amy Chow, Andrea Cerase, Patrick McDonel and Mitchell Guttman

Science **354** (6311), 468-472.
DOI: 10.1126/science.aae0047originally published online August 4, 2016

Plunging into a domain of silence

Female mammals have two X chromosomes. One must be silenced to "balance" gene dosage with male XY cells. The Xist long noncoding RNA coats the inactive X chromosome in female mammalian cells. Chen *et al.* show that the Xist RNA helps recruit the X chromosome to the internal rim of the cell nucleus, a region where gene expression is silenced. Xist is recruited to the domain through an interaction with the Lamin B receptor. This recruitment allows the Xist RNA to spread across the future inactive X chromosome, shutting down gene expression.

Science, this issue p. 468